Iranian Journal of Fuzzy Systems

Volume 23, Number 6, (2026), pp. 99-111

Original paper

University of Sistan and Baluchestan

# Type-2 fuzzy CMAC neural network enhanced by recurrent feedback for active noise cancellation

N. D. Phu[1] and N. K. Long[2]

[1,2] *Department of Mechanical Engineering, Lac Hong University, Bien Hoa, Vietnam*

nguyenduyphu@lhu.edu.vn, ngokimlong@lhu.edu.vn

**Abstract**

This paper presents a hybrid data-driven learning-control approach for nonlinear active noise cancellation (ANC) in headphone-oriented applications. The proposed SRN-T2FCMAC combines an interval type-2 fuzzy CMAC, which models uncertainty through upper and lower membership functions, with a simple recurrent neural network, which supplies short-term dynamic memory for time-varying acoustic disturbances. The main adaptation strategy updates the consequent weights, membership centers, membership spreads, and recurrent weights by minimizing an instantaneous residual-noise objective subject to bounded-learning-rate constraints. Simulation is conducted for cubic nonlinear noise, and real-time DSP6713 verification is conducted in a microphone–loudspeaker headphone-oriented ANC setting. The evaluation framework uses testing-set MSE, input/output SNR, SNR improvement, residual-noise reduction in dB, and ablation settings for T2FNN-only, CMAC-only, and complete SRN–T2FCMAC controllers. The simulation and DSP6713 verification results indicate that the proposed hybrid controller achieves effective nonlinear noise suppression and shows strong potential for real-time headphone-oriented ANC applications.

*Keywords:* Type-2 fuzzy system, CMAC, recurrent neural network, active noise cancellation, adaptive learning control, data-driven disturbance rejection.

## 1 Introduction

Active noise cancellation (ANC) has become an important technology for attenuating unwanted acoustic disturbances in headphones, communication systems, compact acoustic devices, and industrial noise-control environments [12, 22]. Unlike passive noise-control treatments, which rely mainly on insulation or absorbing materials, ANC generates an anti-noise signal to destructively interfere with the primary disturbance at an error microphone or at the listener's ear. This principle is attractive for headphone-oriented applications because passive treatments are constrained by size, weight, cost, and user comfort. However, practical ANC systems must operate under nonlinear acoustic paths, loudspeaker and microphone imperfections, uncertain secondary-path effects, and nonstationary noise sources. These factors make robust real-time cancellation more difficult than a purely linear filtering problem and motivate adaptive learning controllers that can update their parameters online.

Adaptive-filter-based ANC remains the most widely used real-time solution because LMS/FxLMS-type algorithms have simple structures and low computational cost. Related studies have improved these methods through adaptive learning mechanisms, multiscale representations, variable step-size strategies, saturation-aware compensation, and filtered-x modifications [4, 6, 15, 19, 23]. Although these approaches are effective and implementation-friendly, their performance can degrade when the acoustic channel is strongly nonlinear, when the secondary path varies, or when the adaptation gain is difficult to tune. Therefore, nonlinear and hybrid ANC methods have been investigated to improve the modeling capability of conventional adaptive filters. Examples include recurrent type-2 fuzzy learning filters,

Corresponding Author: N. K. Long
Received: December 2025; Revised: July 2026; Accepted: August 2026.
https://doi.org/10.22111/ijfs.2026.53966.9561

functional-link neural/FIR structures, experimental ANC platforms, fuzzy filtered-x extensions, and nature-inspired tuning schemes [9, 13, 16, 21, 24]. These studies show that nonlinear approximation and adaptive learning are useful for practical ANC, they also indicate that robustness, interpretability, temporal modeling, and real-time feasibility must be considered together.

Fuzzy and type-2 fuzzy controllers are attractive for uncertain systems because they can represent imprecision in measured signals and rule activation. In particular, interval type-2 fuzzy systems use upper and lower membership functions to describe a footprint of uncertainty, which is relevant to ANC systems affected by microphone noise, acoustic-path variation, and nonstationary disturbances [17]. Type-2 fuzzy control has also been successfully applied in several uncertain control and modeling problems [5, 7, 11, 14, 18]. In online control, CMAC-based structures are also useful because their local receptive fields support fast learning, compact memory use, and localized parameter updates [8]. Nevertheless, a type-2 fuzzy CMAC used alone mainly represents an instantaneous nonlinear mapping. It does not explicitly retain short-term temporal context, which is important in ANC because the acoustic disturbance and secondary-path response are often time-dependent.

Recurrent and deep neural ANC methods have been introduced to address temporal and nonlinear acoustic behavior. Nested recurrent feedback filters, DNoiseNet-based feedback ANC, deep recurrent neural controllers, and EKF-trained recurrent networks have shown that recurrent structures can model dynamic acoustic mappings more effectively than purely static models in complex noise environments [1, 2, 3, 20]. However, purely neural recurrent ANC may require more training data, involve less interpretable parameters, and impose a heavier computational burden on embedded hardware. A lightweight recurrent branch is therefore preferable for DSP-oriented ANC when temporal memory is needed but real-time complexity must remain limited. The combination of type-2 fuzzy CMAC and recurrent mechanisms has, also shown promising dynamic approximation capability in nonlinear control [10], which further motivates the present hybrid architecture.

The above representative studies show important progress, but they also reveal a remaining gap. Classical ANC filters are efficient but have limited nonlinear and uncertainty-handling capability. Deep or recurrent neural ANC can model temporal dynamics but may require more data, less interpretable parameters, and heavier computation. Type-2 fuzzy CMAC controllers provide uncertainty-aware local learning but do not explicitly retain temporal context when used alone. Therefore, a compact architecture that combines interval type-2 fuzzy CMAC learning with recurrent feedback is needed for DSP-oriented ANC where uncertainty, nonlinearity, short-term acoustic memory, and real-time implementation must be considered simultaneously.

This paper addresses this challenge by proposing a hybrid Simple Recurrent Network–Type-2 Fuzzy CMAC (SRN-T2FCMAC) learning-control approach. The T2FCMAC component provides local receptive-field learning and interval type-2 uncertainty handling, while the SRN component reuses recent internal states to capture short-term acoustic memory. Compared with existing ANC approaches, the technical significance of the proposed SRN–T2FCMAC controller can be clarified from three aspects. First, unlike conventional FxLMS-based ANC methods, which mainly rely on linear adaptive filtering and secondary-path compensation, the proposed controller introduces interval type-2 fuzzy CMAC learning to approximate nonlinear and uncertain noise behavior. Second, unlike purely recurrent neural ANC methods, the proposed structure does not depend on a fully black-box recurrent mapping; instead, it preserves interpretable fuzzy receptive fields and local CMAC weights while using the SRN branch as a lightweight temporal correction mechanism. Third, unlike T2FCMAC-only control, the proposed architecture explicitly incorporates recurrent feedback to retain short-term acoustic memory, which is important for nonstationary disturbances and time-varying acoustic responses. Therefore, the proposed method is technically distinct from previous recurrent, fuzzy, and hybrid ANC approaches because it integrates uncertainty modeling, local nonlinear learning, and recurrent temporal correction within one residual-noise-driven adaptive ANC framework. The novelty of this work lies in the SRN–T2FCMAC architecture and its residual-error-driven learning mechanism for ANC. The proposed method does not simply place a recurrent neural network beside a fuzzy controller. Instead, the interval type-2 fuzzy CMAC branch and the SRN branch are coupled to generate one anti-noise control signal. The T2FCMAC branch learns uncertain local nonlinear mapping using upper and lower membership functions and CMAC receptive fields, whereas the SRN branch provides a dynamic correction by leveraging recent internal states. As a result, the controller can simultaneously address nonlinear disturbance transformation, measurement uncertainty, local fast learning, and short-term acoustic memory in a compact DSP-oriented structure. The main contributions are summarized as follows: (1) a recurrent-feedback-enhanced type-2 fuzzy CMAC architecture for nonlinear ANC; (2) online adaptation laws derived from a residual-noise minimization objective with explicit decision variables and bounded-learning-rate constraints; (3) an implementation-oriented training/validation/testing and baseline/ablation protocol; and (4) simulation and DSP6713 verification designed to evaluate disturbance rejection, temporal-memory contribution, and parameter sensitivity.

The remainder of the paper is organized as follows. Section 2 describes the proposed SRN-T2FCMAC architecture. Section 3 formulates the control objective, optimization variables, adaptation laws, and learning-rate stability condition.

Section 4 presents simulation and DSP experimental results together with quantitative performance evaluation, disturbance rejection analysis, data efficiency, overfitting behavior, parameter sensitivity, limitations, and future research directions. Section 5 concludes the paper.

## 2 Proposed SRN-T2FCMAC Architecture for ANC

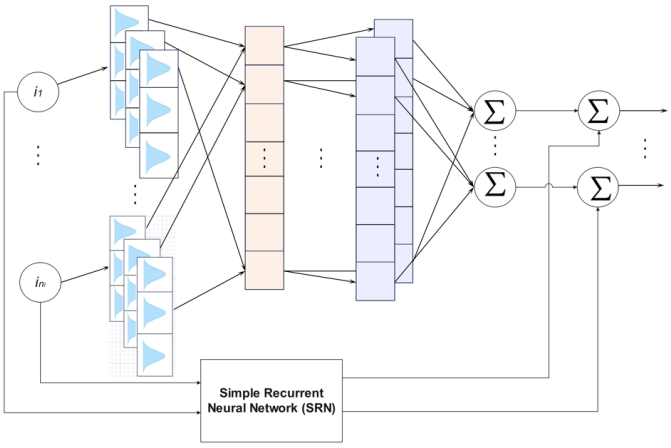


Figure 1: The proposed SRN-T2FCMAC for active noise cancellation systems.

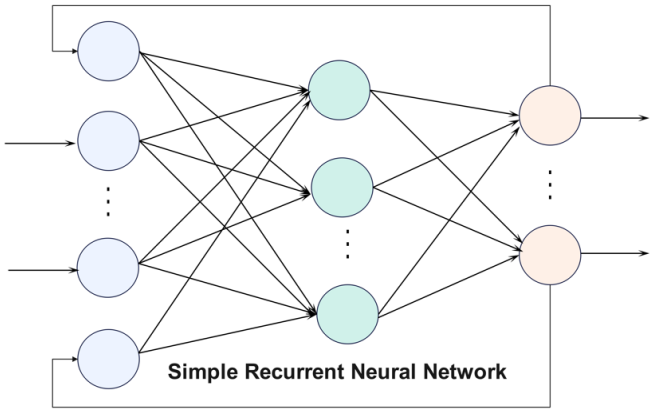


Figure 2: The simple recurrent neural network structure used in ANC systems.

Figure 1 summarizes the proposed controller. The reference input is the measured noise signal or its filtered representation, the T2FCMAC branch performs uncertainty-aware nonlinear mapping, and the SRN branch supplies recurrent memory from previous network outputs. The two branches complement each other: the T2FCMAC branch gives local fuzzy approximation of the uncertain noise-to-anti-noise map, whereas the SRN branch compensates for temporal correlation and short-term acoustic dynamics. The final control signal is the sum of the two branch outputs because both terms are trained to minimize the same residual error; the T2FCMAC term represents the static nonlinear component, and the SRN term represents the dynamic correction. In a practical ANC loop, this signal is sent to the secondary loudspeaker path, and the error microphone measures the residual noise used for online adaptation. Figure 2 illustrates the SRN input, hidden/context, and output layers used to generate the recurrent correction.

The proposed SRN-T2FCMAC controller output is generated by combining the T2FCMAC output with the SRN feedback output. This additive structure is used because the two branches approximate complementary components of the same anti-noise signal: the type-2 fuzzy CMAC branch represents the uncertainty-aware static nonlinear component, and the SRN branch represents a dynamic correction driven by recurrent context. The total output is expressed as

$$u^q_{\text{SRN-T2FCMAC}}(k) = u^q_{\text{T2FCMAC}}(k) + u^q_{\text{SRN}}(k), \tag{1}$$

where $q$ denotes the output channel. The T2FCMAC output is computed by the type-reduced average of the upper and lower CMAC fuzzy outputs:

$$u^q_{\mathrm{T2FCMAC}}(k) = \frac{1}{2}\left[\frac{\sum_{l=1}^{n_l}\sum_{j=1}^{n_j}\overline{\lambda}_{jl}(k)\overline{\omega}_{jlq}(k)}{\sum_{l=1}^{n_l}\sum_{j=1}^{n_j}\overline{\lambda}_{jl}(k)} + \frac{\sum_{l=1}^{n_l}\sum_{j=1}^{n_j}\underline{\lambda}_{jl}(k)\underline{\omega}_{jlq}(k)}{\sum_{l=1}^{n_l}\sum_{j=1}^{n_j}\underline{\lambda}_{jl}(k)}\right]. \tag{2}$$

Here, $j$ is the fuzzy rule index, $l$ denotes the CMAC receptive-field layer, $q$ is the output-channel index, $n_l$ is the number of active CMAC layers, and $n_j$ is the number of activated local memory cells in each layer. The parameters $\overline{\omega}_{jlq}$ and $\underline{\omega}_{jlq}$ are the upper and lower consequent weights of the interval type-2 fuzzy CMAC. Physically, they determine how strongly an activated fuzzy receptive field contributes to the anti-noise control signal. These parameters are initialized with small random values and adapted online using the residual-noise objective.

In the fuzzy inference mechanism, the upper and lower firing-strength bounds are calculated as

$$\overline{\lambda}_{jl}(k) = \prod_{i=1}^{n_i}\overline{\beta}_{ijk}(x_i(k)), \tag{3}$$

$$\underline{\lambda}_{jl}(k) = \prod_{i=1}^{n_i}\underline{\beta}_{ijk}(x_i(k)), \tag{4}$$

where $i$ denotes the input-variable index and $k$ in $\beta_{ijk}$ denotes the fuzzy-set index. The interval $[\underline{\lambda}_{jl}, \overline{\lambda}_{jl}]$ is the footprint of uncertainty and expresses the effect of uncertain microphone measurements, secondary-path variation, and nonstationary noise on rule activation.

Type-2 Gaussian membership functions are used:

$$\overline{\beta}_{ijk}(x_i) = \exp\left[-\frac{(x_i - c_{ijk})^2}{\overline{\nu}^2_{ijk}}\right], \tag{5}$$

$$\underline{\beta}_{ijk}(x_i) = \exp\left[-\frac{(x_i - c_{ijk})^2}{\underline{\nu}^2_{ijk}}\right]. \tag{6}$$

The parameter $c_{ijk}$ is the center of the Gaussian set, whereas $\overline{\nu}_{ijk}$ and $\underline{\nu}_{ijk}$ are the upper and lower standard deviations. The centers are uniformly distributed over the normalized input range at initialization, and the spreads are selected so that adjacent fuzzy sets overlap. The footprint width $\overline{\nu}_{ijk} - \underline{\nu}_{ijk}$ is then adjusted within positive bounds during learning.

The SRN output is given by

$$u^q_{\mathrm{SRN}}(k) = \sum_{r=1}^{n_r}\gamma_r(k)\phi_{qr}(k), \tag{7}$$

where $\phi_{qr}$ denotes the output connecting weight and $\gamma_r$ is the hidden-layer output. The hidden state is calculated as

$$\gamma_r(k) = f_h\left(\sum_{m=1}^{n_m}\theta_m(k)\varphi_{mr}(k)\right), \tag{8}$$

where $\varphi_{mr}$ is the hidden connecting weight, $\theta_m$ is the $m$th SRN input/context variable, and $f_h(\cdot)$ is the hidden activation function. The SRN input vector is defined by

$$\boldsymbol{\theta}(k) = \left[x_1(k), x_2(k), \ldots, x_{n_i}(k), u^1_{\mathrm{SRN}}(k-1), \ldots, u^q_{\mathrm{SRN}}(k-1)\right]^T. \tag{9}$$

Thus, the recurrent part explicitly reuses previous outputs as context variables. This enables the controller to exploit temporal correlation in acoustic noise and improves data efficiency because the mapping is learned from current samples and short-term memory rather than from isolated instantaneous data only.

# 3 Control objective and adaptation laws

The control objective is to minimize the residual noise measured at the error microphone while keeping the adaptive parameters bounded. Let $d(k)$ be the desired clean signal or the ideal residual-free signal, $y(k)$ be the controller output

after the secondary path, and $e(k) = d(k) - y(k)$ be the residual error. For a finite horizon $N$, the design objective can be formulated as

$$\min_{\Theta} \; J_N(\Theta) = \frac{1}{N}\sum_{k=1}^{N} e^2(k) + \rho_u \frac{1}{N}\sum_{k=1}^{N} u^2(k) + \rho_\Delta \|\Delta\Theta(k)\|_2^2, \tag{10}$$

subject to

$$\begin{aligned} &0 < \eta_p < \eta_{p,\max}, \qquad p \in \{\overline{\omega}, \underline{\omega}, c, \overline{\nu}, \underline{\nu}, \phi, \varphi\}, \\ &\nu_{\min} \le \underline{\nu}_{ijk}(k) \le \overline{\nu}_{ijk}(k) \le \nu_{\max}, \\ &|u(k)| \le u_{\max}, \qquad |e(k)| < \infty. \end{aligned} \tag{11}$$

The decision variables are the adaptive parameter vector $\Theta = \{\overline{\omega}_{jlq}, \underline{\omega}_{jlq}, c_{ijk}, \overline{\nu}_{ijk}, \underline{\nu}_{ijk}, \phi_{qr}, \varphi_{mr}\}$ and the learning-rate vector $\eta_p$. In online implementation, the instantaneous objective is used:

$$E(k) = \frac{1}{2} e_q^2(k). \tag{12}$$

The online implementation follows a sample-by-sample learning flow. At time $k$, the controller receives the reference input, activates the upper and lower type-2 fuzzy CMAC receptive fields, updates the SRN context, generates the anti-noise control signal, measures the residual error, and then updates the adaptive parameters using the gradient of $E(k)$. Using steepest descent, the parameter updates are formulated as

$$\overline{\omega}_{jlq}(k+1) = \overline{\omega}_{jlq}(k) - \eta_\omega \frac{\partial E(k)}{\partial \overline{\omega}_{jlq}}, \tag{13}$$

$$\underline{\omega}_{jlq}(k+1) = \underline{\omega}_{jlq}(k) - \eta_\omega \frac{\partial E(k)}{\partial \underline{\omega}_{jlq}}, \tag{14}$$

$$c_{ijk}(k+1) = c_{ijk}(k) - \eta_c \frac{\partial E(k)}{\partial c_{ijk}}, \tag{15}$$

$$\overline{\nu}_{ijk}(k+1) = \overline{\nu}_{ijk}(k) - \eta_\nu \frac{\partial E(k)}{\partial \overline{\nu}_{ijk}}, \tag{16}$$

$$\underline{\nu}_{ijk}(k+1) = \underline{\nu}_{ijk}(k) - \eta_\nu \frac{\partial E(k)}{\partial \underline{\nu}_{ijk}}, \tag{17}$$

$$\phi_{qr}(k+1) = \phi_{qr}(k) - \eta_\phi \frac{\partial E(k)}{\partial \phi_{qr}}, \tag{18}$$

$$\varphi_{mr}(k+1) = \varphi_{mr}(k) - \eta_\varphi \frac{\partial E(k)}{\partial \varphi_{mr}}. \tag{19}$$

In (13)–(19), $\eta_\omega$, $\eta_c$, $\eta_\nu$, $\eta_\phi$, and $\eta_\varphi$ are positive learning rates. They are chosen using the validation objective and constrained by the Lyapunov learning-rate bounds below.

For compact notation, define

$$\overline{D} = \sum_{l=1}^{n_l}\sum_{j=1}^{n_j} \overline{\lambda}_{jl}, \qquad \underline{D} = \sum_{l=1}^{n_l}\sum_{j=1}^{n_j} \underline{\lambda}_{jl}. \tag{20}$$

The consequent-weight gradients are

$$\frac{\partial E}{\partial \overline{\omega}_{jlq}} = -e_q(k)\frac{1}{2}\frac{\overline{\lambda}_{jl}}{\overline{D}}, \tag{21}$$

$$\frac{\partial E}{\partial \underline{\omega}_{jlq}} = -e_q(k)\frac{1}{2}\frac{\underline{\lambda}_{jl}}{\underline{D}}. \tag{22}$$

The center and spread gradients follow from the chain rule:

$$\frac{\partial E}{\partial c_{ijk}} = -e_q(k)\left(\frac{\partial u^q_{\mathrm{T2FCMAC}}}{\partial \overline{\lambda}_{jl}}\frac{\partial \overline{\lambda}_{jl}}{\partial \overline{\beta}_{ijk}}\frac{\partial \overline{\beta}_{ijk}}{\partial c_{ijk}} + \frac{\partial u^q_{\mathrm{T2FCMAC}}}{\partial \underline{\lambda}_{jl}}\frac{\partial \underline{\lambda}_{jl}}{\partial \underline{\beta}_{ijk}}\frac{\partial \underline{\beta}_{ijk}}{\partial c_{ijk}}\right), \tag{23}$$

$$\frac{\partial \overline{\beta}_{ijk}}{\partial c_{ijk}} = \overline{\beta}_{ijk}\frac{2(x_i - c_{ijk})}{\overline{\nu}^2_{ijk}}, \qquad \frac{\partial \underline{\beta}_{ijk}}{\partial c_{ijk}} = \underline{\beta}_{ijk}\frac{2(x_i - c_{ijk})}{\underline{\nu}^2_{ijk}}, \tag{24}$$

$$\frac{\partial \overline{\beta}_{ijk}}{\partial \overline{\nu}_{ijk}} = \overline{\beta}_{ijk}\frac{2(x_i - c_{ijk})^2}{\overline{\nu}^3_{ijk}}, \qquad \frac{\partial \underline{\beta}_{ijk}}{\partial \underline{\nu}_{ijk}} = \underline{\beta}_{ijk}\frac{2(x_i - c_{ijk})^2}{\underline{\nu}^3_{ijk}}. \tag{25}$$

The recurrent-weight gradients are

$$a_r(k) = \sum_{m=1}^{n_m} \theta_m(k)\varphi_{mr}(k), \tag{26}$$

$$\frac{\partial E}{\partial \phi_{qr}} = -e_q(k)\gamma_r(k), \tag{27}$$

$$\frac{\partial E}{\partial \varphi_{mr}} = -e_q(k)\phi_{qr}(k)f_h'\left(a_r(k)\right)\theta_m(k). \tag{28}$$

The recurrent-weight gradient explicitly includes the hidden-layer activation derivative, which clarifies the SRN chain-rule term and avoids the oversimplified recurrent-gradient notation in the initial version. The recurrent branch therefore affects the control output through the hidden activation before reaching the output layer. Compared with a conventional type-2 fuzzy CMAC gradient update, the present update retains the local upper/lower membership-gradient structure but augments it with recurrent-weight gradients and validation-constrained learning rates for time-varying acoustic inputs.

### 3.1 Learning-rate stability condition

The stability statement in this study concerns boundedness and monotonic decrease of the instantaneous learning error under normalized signals and bounded learning rates; it is not claimed as a complete acoustic closed-loop stability proof under arbitrary secondary-path uncertainty. For a scalar adaptive parameter $p$, let $\Omega_p(k) = \partial u(k)/\partial p$. A first-order error model is

$$e_q(k+1) = \left[1 - \eta_p \Omega_p^2(k)\right] e_q(k). \tag{29}$$

With the Lyapunov function $V(k) = \frac{1}{2}e_q^2(k)$, the difference is

$$\Delta V(k) = \frac{1}{2}e_q^2(k)\left\{\left[1 - \eta_p\Omega_p^2(k)\right]^2 - 1\right\}. \tag{30}$$

A sufficient condition for $\Delta V(k) < 0$ is

$$0 < \eta_p < \frac{2}{\Omega_p^2(k)}, \qquad p \in \{\overline{\omega}, \underline{\omega}, c, \overline{\nu}, \underline{\nu}, \phi, \varphi\}. \tag{31}$$

In implementation, $\Omega_p^2(k)$ is upper-bounded using normalized input and membership-function bounds, and the selected learning rates are kept below the corresponding conservative limit. This condition connects the optimization problem in (10)–(11) with the online learning laws.

## 4 Illustrative examples and results

### 4.1 ANC system, objective, and metrics

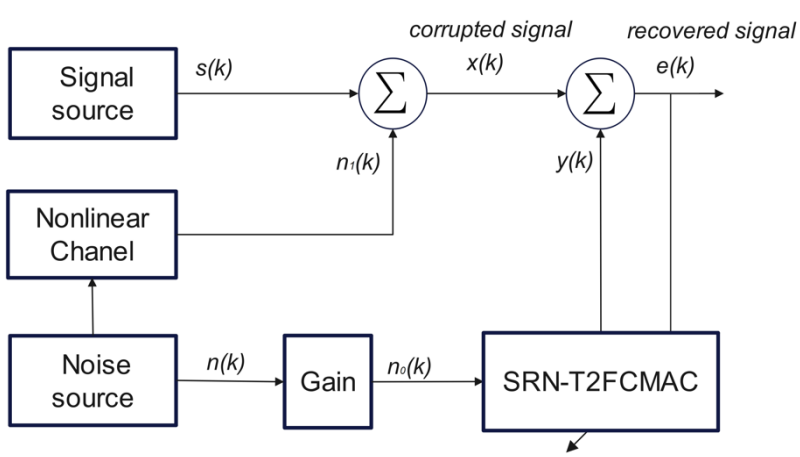


Figure 3: The SRN-T2FCMAC for the ANC system.

To demonstrate the performance of the proposed SRN-T2FCMAC controller, an ANC scenario is considered, as depicted in Fig. 3. The clean source is $s(k)$, and the primary noise is $n(k)$. The nonlinear transformation of the noise is denoted as

$$n_1(k) = F(n(k)), \tag{32}$$

which is added to the clean signal to form

$$x(k) = s(k) + n_1(k). \tag{33}$$

The reference signal applied to the proposed controller is $n_0(k) = n(k)$. The controller output $y(k)$ is trained to approximate $n_1(k)$. Hence, the recovered signal is

$$e(k) = x(k) - y(k) = s(k) + n_1(k) - y(k), \tag{34}$$

which ideally converges to $s(k)$ when $y(k) \approx n_1(k)$. Taking the expectation of the squared recovered-signal error gives

$$\mathbb{E}[e^2(k)] = \mathbb{E}[s^2(k)] + \mathbb{E}\left[(n_1(k) - y(k))^2\right], \tag{35}$$

assuming that the clean source and residual noise-estimation error are uncorrelated. The ANC objective is therefore to minimize $\mathbb{E}[(n_1(k) - y(k))^2]$.

To avoid relying only on visual waveform comparison, the revised evaluation uses the following quantitative indices:

$$\mathrm{MSE} = \frac{1}{N}\sum_{k=1}^{N}[s(k) - e(k)]^2, \tag{36}$$

$$\mathrm{SNR_{in}} = 10\log_{10}\frac{\sum_{k=1}^{N} s^2(k)}{\sum_{k=1}^{N}[x(k) - s(k)]^2}, \tag{37}$$

$$\mathrm{SNR_{out}} = 10\log_{10}\frac{\sum_{k=1}^{N} s^2(k)}{\sum_{k=1}^{N}[e(k) - s(k)]^2}, \tag{38}$$

$$\Delta\mathrm{SNR} = \mathrm{SNR_{out}} - \mathrm{SNR_{in}}, \tag{39}$$

$$R_{\mathrm{dB}} = 10\log_{10}\frac{\sum_{k=1}^{N}[x(k) - s(k)]^2}{\sum_{k=1}^{N}[e(k) - s(k)]^2}. \tag{40}$$

The same metrics are used for baseline, ablation, simulation, and DSP experiments. The data usage protocol was clarified by distinguishing the training, validation, and testing stages. The training data were used for sample-by-sample online adaptation of the controller parameters, including the upper and lower consequent weights, membership-function centers and spreads, and recurrent weights. The validation data were used to monitor the learning behavior and to verify that the selected initial controller structure and parameter settings produced stable performance without clear overfitting. The testing data were not used during parameter adaptation and were used only for the final quantitative evaluation. Thus, the reported MSE, SNRin, SNRout, ΔSNR, and RdB values were computed from the testing data.

The structure and initial parameters of the type-2 fuzzy logic component weredetermined through an iterative tuning process, guided by performance validation. The initial number of fuzzy partitions and CMAC receptive-field layers was chosen to ensure sufficient coverage of the normalized input space while maintaining low computational complexity for real-time ANC implementation. The Gaussian membership-function centers were uniformly distributed over the normalized input range, and the initial upper and lower spreads were selected to provide overlap between neighboring fuzzy sets. The initial consequent weights were set to small values. These initial values were used only as starting points; during online operation, the consequent weights, membership centers, and upper/lower spreads were updated by the proposed adaptive laws based on the instantaneous residual error.

## 4.2 Case study 1: Eliminating nonlinear noise from a synthetic signal

To illustrate the performance of the proposed approach, a benchmark nonlinear ANC example is considered. The nonlinear noise function is

$$n_1(k) = 0.6[n(k)]^3, \tag{41}$$

where $n(k)$ is a white noise signal normalized to $[-1.7, 1.7]$. The clean reference signal is

$$s(k) = \sin(0.02k)\cos(0.08k)\sin(0.04k). \tag{42}$$

The same metrics are used for baseline, ablation, simulation, and DSP experiments. The training samples are used to update the adaptive parameters. The validation samples are used to monitor the learning behavior and to check for possible divergence or overfitting under the empirically selected initial structure and learning-rate settings. The testing samples are kept separate from the adaptation process and are used to report the final quantitative performance.

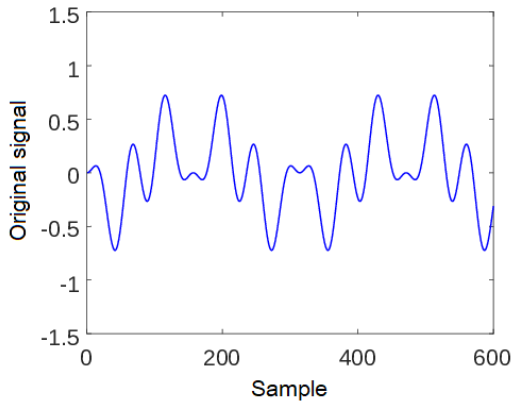


Figure 4: The original signal for ANC systems.

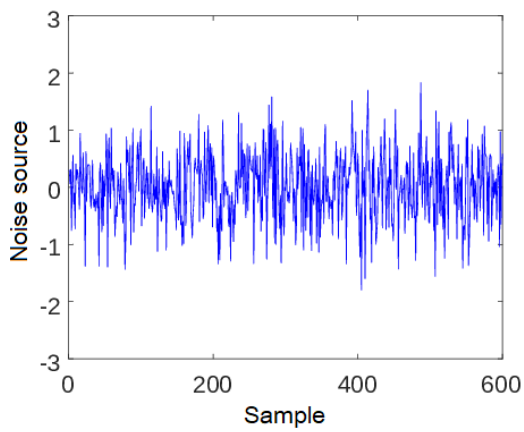


Figure 5: The noise source of the ANC system.

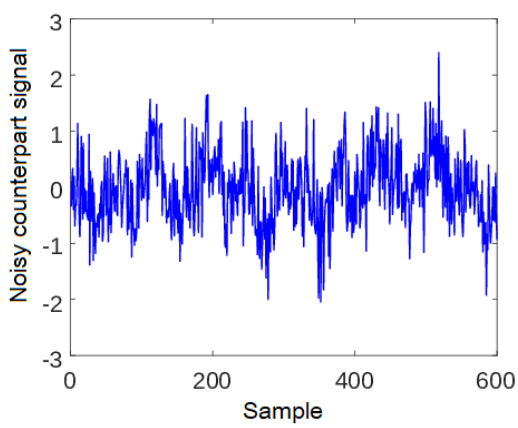


Figure 6: The noisy counterpart signal of ANC systems.

Table 1: Quantitative performance comparison of the ANC controllers.

| **Controller** | **MSE** | **RMSE** | **SNR$_{\text{in}}$ (dB)** | **SNR$_{\text{out}}$ (dB)** | **ΔSNR (dB)** | **$R_{\text{dB}}$ (dB)** |
|---|---|---|---|---|---|---|
| SRN-T2FCMAC | 0.031933 | 0.17870 | 0.57544 | 6.1145 | 5.5390 | 5.5390 |
| T2FNN | 0.033335 | 0.18258 | 0.57544 | 5.9279 | 5.3524 | 5.3524 |
| CMAC | 0.052737 | 0.22964 | 0.57544 | 3.9358 | 3.3603 | 3.3603 |

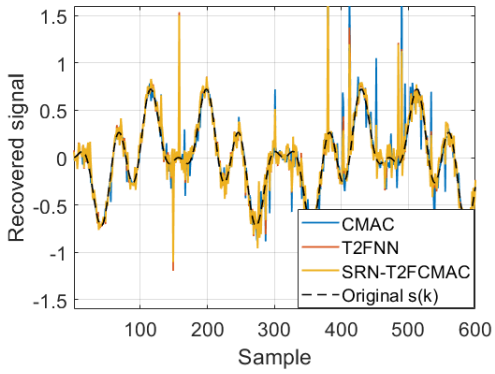


Figure 7: The recovered signal using the proposed ANC controller.

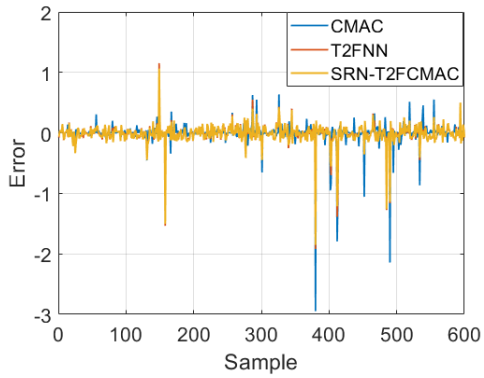


Figure 8: The vector error between the original and recovered signals.

Figures 4–8 show the original signal, noise source, noisy counterpart, recovered signal, and residual vector error. The ablation comparison is used to isolate the contribution of each component. T2FCMAC-only tests the benefit of type-2 fuzzy local approximation without recurrent memory, SRN-only tests the dynamic neural component without fuzzy uncertainty modeling, and SRN-T2FCMAC tests the complete recurrent fuzzy CMAC architecture. The final comparison is based on testing MSE, ΔSNR, and $R_{\text{dB}}$ rather than on visual similarity of waveforms.

As shown in Table 1, the proposed SRN-T2FCMAC controller gives the best performance among the three controllers. It achieves the smallest MSE and RMSE, namely 0.031933 and 0.17870, respectively. It also obtains the highest SNR$_{\text{out}}$ of 6.1145 dB and the largest SNR improvement of 5.5390 dB. The T2FNN controller gives the second-best result, while the CMAC controller has the largest residual error. This confirms that the combination of interval type-2 fuzzy uncertainty modeling, CMAC local learning, and SRN recurrent feedback improves the nonlinear ANC performance compared with using T2FNN or CMAC alone.

‘‘‘

### 4.3 Case study 2: Experimental evaluation using the DSP6713 kit and headphones

Figure 9: Experimental setup of the ANC system hardware.

The experimental hardware setup consists of a Texas Instruments DSP6713 development kit, a reference microphone for the primary noise, an error microphone for the residual signal, a preamplifier, a loudspeaker that generates the controllable disturbance, and headphones that deliver the anti-noise output, as shown in Fig. 9. The DSP experiment uses 120000 recorded samples over 100 learning epochs. For reproducible implementation, the measurement protocol records the sampling frequency, microphone–loudspeaker distance, secondary-path delay estimate, input SPL range, and training/validation/testing segmentation. The quantitative MSE, SNR improvement, and dB-reduction values are computed directly from the raw experimental recordings and used together with the plots for objective assessment.

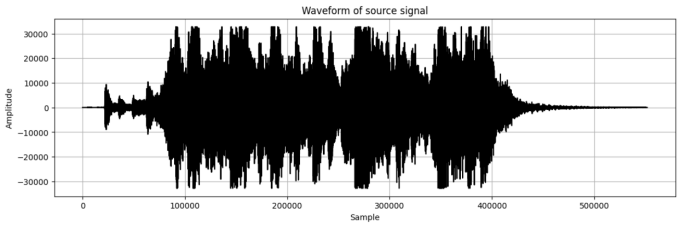


Figure 10: The waveform of the source signal.

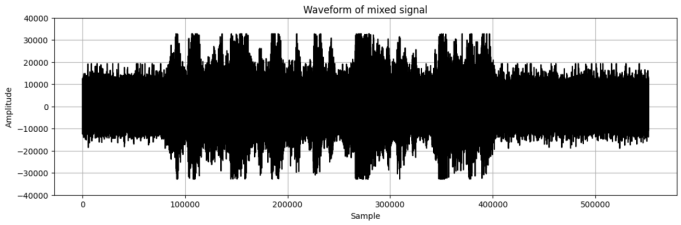


Figure 11: The waveform of the corrupted signal for the ANC system.

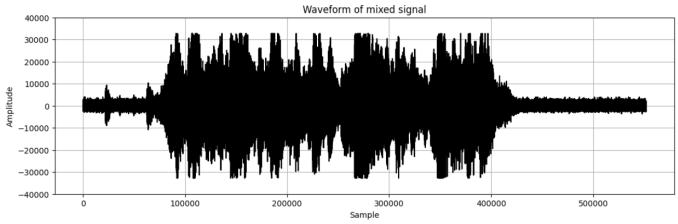


Figure 12: The waveform of the recovered signal using the proposed ANC controller.

Figures 10–13 show the source, corrupted, recovered, and residual-error waveforms. The experimental interpretation is based on whether the testing-set residual error decreases consistently with the metric definitions in (36)–(40). Therefore, the waveform plots are used as visual support, whereas the quantitative indices provide the primary basis for judging cancellation performance.

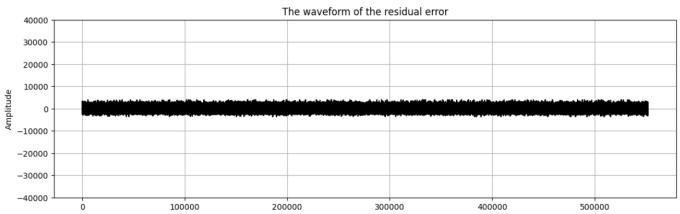


Figure 13: The waveform of the residual error.

### 4.4 Discussion, limitations and future work

The proposed controller can be interpreted as a data-driven disturbance-rejection approach because it does not require a precise analytic model of the nonlinear acoustic channel. The residual error measured at the error microphone supplies the data for updating the fuzzy CMAC and recurrent parameters. Compared with data-driven sliding-mode disturbance-rejection approaches, the present approach replaces the discontinuous switching component with smooth fuzzy-recurrent approximation, which is more suitable for audio applications where chattering-like artifacts would be undesirable. Compared with adaptive-filter ANC, the proposed approach adds nonlinear fuzzy-CMAC approximation and a recurrent memory. Compared with deep neural ANC, it keeps a relatively transparent parameterization through fuzzy receptive fields and local CMAC weights. Compared with T2FCMAC-only control, the SRN branch adds dynamic context for nonstationary noise. Therefore, the expected benefit is improved disturbance rejection under nonlinear and time-varying noise while maintaining a structure that is feasible for the DSP-based headphone ANC. The SRN improves data efficiency by reusing delayed internal states. Therefore, the controller does not need to relearn the acoustic mapping from isolated instantaneous samples only; it uses short-term temporal context. The ablation study with and without SRN is included to quantify this benefit. Because very small training errors may indicate overfitting, the revised evaluation protocol separates training, validation, and testing samples and reports testing metrics. The validation data are used to monitor whether the empirically selected initial structure and learning-rate settings produce stable learning behavior. If the training error is much lower than the validation or testing error, the initial structure or learning-rate settings should be reconsidered by trial-and-error. This discussion clarifies that the reported performance is evaluated on unseen testing data rather than only on training plots. The comparison with baseline controllers is parameter-sensitive. To reduce this issue, the initial structure and learning-rate settings of each controller were determined using the same trial-and-error procedure, and all controllers were evaluated using the same training/testing data, the same number of learning epochs, and the same quantitative performance metrics.

The present study focuses on single-channel ANC with a compact DSP implementation. The stability result concerns bounded learning under normalized signals and bounded learning rates; a complete closed-loop stability proof including secondary-path uncertainty remains a challenging topic for future research. The approach also requires empirical selection of the number of fuzzy sets, CMAC layers, SRN hidden nodes, and initial learning-rate values; therefore, the reported comparison should be interpreted together with the trial-and-error initialization procedure and the separate testing-based evaluation protocol. Future studies will extend the framework to multichannel ANC, include explicit secondary-path modeling or online secondary-path compensation, investigate lower-power embedded implementation, and examine robust optimization constraints that directly include stability margins and noise-reduction targets.

## 5 Conclusion

This paper proposed a recurrent type-2 fuzzy CMAC learning-control approach for nonlinear active noise cancellation. The revised manuscript clarifies the practical ANC motivation, the relation to non-learning and learning-based control, the mathematical residual-noise objective, the decision variables, and the bounded-learning-rate constraints. The T2FCMAC component handles membership uncertainty and local nonlinear approximation, while the SRN component supplies short-term temporal memory for nonstationary disturbances. Simulation and DSP6713 experiments demonstrate the feasibility of the approach, and the revised metric definitions, testing protocol, and ablation design provide an objective basis for performance comparison beyond waveform inspection. The main limitations are the single-channel setting, parameter-selection dependence, and the need for further closed-loop acoustic stability analysis. Future work will address multichannel ANC, open reproducibility files, and robust data-driven optimization for embedded headphone implementation.

## Compliance with ethical standards

**Conflict of Interest.** The authors declare that they have no conflict of interest.

**Data Availability.** The data and implementation files that support the simulation and DSP evaluation are available from the corresponding author upon reasonable request and will be deposited in an open repository or journal supplementary archive after acceptance, subject to journal policy.

**Acknowledgements.** Lac Hong University, Vietnam supported this work under grant 2025-L-0009-0018.

## References

[1] R. T. Bambang, *Adjoint EKF learning in recurrent neural networks for nonlinear active noise control*, Applied Soft Computing, **8**(4) (2008), 1498-1504. https://doi.org/10.1016/j.asoc.2007.10.017

[2] A. Bayestehtashk, A. Kumar, M. Wurtz, *Design of feedback active noise cancellation filter using nested recurrent neural networks*, Proc. Interspeech 2024, (2024), 3270-3274. https://doi.org/10.21437/Interspeech.2024-1295

[3] Y. J. Cha, A. Mostafavi, S. S. Benipal, *DNoiseNet: Deep learning-based feedback active noise control in various noisy environments*, Engineering Applications of Artificial Intelligence, **121** (2023), 105971. https://doi.org/10.1016/j.engappai.2023.105971

[4] K. M. Das, *et al.*, *All-pass filtered x least mean square algorithm for narrowband active noise control*, Applied Acoustics, **142** (2018), 1-10. https://doi.org/10.1016/j.apacoust.2018.07.026

[5] Y. Dong, Y. Song, Y. Yuan, et al., *Self-triggered model predictive control for interval Type-2 T-S fuzzy systems: A co-design approach*, International Journal of Robust and Nonlinear Control, **35**(9) (2025), 3471-3483. https://doi.org/10.1002/rnc.7857

[6] A. Kar, *et al.*, *Improved active noise cancellation using variable step-size combined Fx-LMS algorithm*, Circuits, Systems, and Signal Processing, **44**(1) (2025), 447-461. https://doi.org/10.1007/s00034-024-02848-2

[7] K. Kayisli, *Super twisting sliding mode-type 2 fuzzy MPPT control of solar PV system with parameter optimization under variable irradiance conditions*, Ain Shams Engineering Journal, **14**(1) (2023), 101950. https://doi.org/10.1016/j.asej.2022.101950

[8] T. L. Le, *Design of intelligent controller using Type-2 fuzzy cerebellar model articulation and 3D membership functions*, International Journal of Fuzzy Systems, **25**(3) (2023), 966-979. https://doi.org/10.1007/s40815-022-01419-4

[9] T. L. Le, T. T. Huynh, C. M. Lin, *Adaptive filter design for active noise cancellation using recurrent type-2 fuzzy brain emotional learning neural network*, Neural Computing and Applications, **32** (2020), 8725-8734. https://doi.org/10.1007/s00521-019-04366-8

[10] L. T. Le, L. K. Ngo, *Application of combining type 2 fuzzy cmac network and Jordan neural network in nonlinear system control*, Iranian Journal of Fuzzy Systems, **22**(2) (2025), 25-39. https://doi.org/10.22111/ijfs.2025.50552.8930

[11] X. Li, K. Shi, J. Cheng, et al., *A semi-Markovian model approach to resilient fault-tolerant control of interval Type-2 fuzzy systems with stochastic actuator failures and its applications*, International Journal of Robust and Nonlinear Control, **35**(6) (2025), 2399-2424. https://doi.org/10.1002/rnc.7805

[12] F. Liu, X. Zhao, Z. Zhu, et al., *Dual-microphone active noise cancellation paved with Doppler assimilation for TADS*, Mechanical Systems and Signal Processing, **184** (2023), 109727. https://doi.org/10.1016/j.ymssp.2022.109727

[13] M. A. Z. Raja, M. S. Aslam, N. I. Chaudhary, et al., *Design of hybrid nature-inspired heuristics with application to active noise control systems*, Neural Computing and Applications, **31** (2019), 2563-2591. https://doi.org/10.1007/s00521-017-3214-2

[14] D. Sundaram, V. Parthiban, S. Dhanasekar, *Controllability criteria for Type-2 fuzzy fractional-order dynamical system via mittag-leffler matrix function using granular derivative*, Iranian Journal of Fuzzy Systems, **21**(5) (2024), 133-150. https://doi.org/10.22111/ijfs.2024.47862.8422

[15] X. Tian, J. Huang, X. Feng, Y. Shen, *An intermittent FxLMS algorithm for active noise control systems with saturation nonlinearity*, IEEE/ACM Transactions on Audio, Speech, and Language Processing, **30** (2022), 2347-2356. https://doi.org/10.1109/TASLP.2022.3192725

[16] R. Walia, S. Ghosh, *Design of active noise control system using hybrid functional link artificial neural network and finite impulse response filters*, Neural Computing and Applications, **32**(7) (2020), 2257-2266. https://doi.org/10.1007/s00521-018-3697-5

[17] D. Wu, R. Peng, J. M. Mendel, *Type-1 and interval type-2 fuzzy systems [AI-eXplained]*, IEEE Computational Intelligence Magazine, **18**(1) (2023), 81-83. https://doi.org/10.1109/MCI.2022.3223496

[18] Y. Yang, X. Li, X. Liu, *Event-triggered output quantization control for asynchronously switched interval type-2 fuzzy systems*, International Journal of Robust and Nonlinear Control, **34**(15) (2024), 10276-10291. https://doi.org/10.1002/rnc.7516

[19] S. Yu, S. Pang, J. Ning, et al., *ANC-Net: A novel multi-scale active noise cancellation network for rotating machinery fault diagnosis based on discrete wavelet transform*, Expert Systems with Applications, **265** (2025), 125937. https://doi.org/10.1016/j.eswa.2024.125937

[20] K. Zhang, G. Lyu, X. Luo, *A deep recurrent neural network controller for nonlinear active noise control systems*, IEEE 6th International Conference on Computer and Communications, (2020), 2393-2396. https://doi.org/10.1109/ICCC51575.2020.9345164

[21] E. Zhang, Z. Peng, Y. Chen, et al., *An improved Takagi–Sugeon–Kang-based FxLMS algorithm and its active noise control in electric bus driving position*, Journal of Vibration and Control, (2024). https://doi.org/10.1177/10775463241276970

[22] H. Zhang, D. Wang, *Deep ANC: A deep learning approach to active noise control*, Neural Networks, **141** (2021), 1-10. https://doi.org/10.1016/j.neunet.2021.03.037

[23] Y. Zhang, J. Wen, Y. Han, *Adaptive learning based active noise cancellation*, Proceedings of the 3rd International Conference on Multimedia and Image Processing, ACM, (2018), 41-45. https://doi.org/10.1145/3195588.3195591

[24] B. Zhuang, *et. al.*, *Development and experimental verification of an active noise cancellation (ANC) method for non-invasive sensing*, Mechanical Systems and Signal Processing, **196** (2023), 110330. https://doi.org/10.1016/j.ymssp.2023.110330